PHYSICAL REVIEW D **82,** 074503 (2010)

Evidence for a conformal phase in SU(N) gauge theories

A. Deuzeman,[1] M. P. Lombardo,[2] and E. Pallante[1]
[1]*Centre for Theoretical Physics, University of Groningen, 9747 AG, Netherlands*
[2]*INFN-Laboratori Nazionali di Frascati, I-00044, Frascati (Rome), Italy*
(Received 27 May 2009; revised manuscript received 21 May 2010; published 18 October 2010)

We discuss the existence of a conformal phase in SU(N) gauge theories in four dimensions. In this lattice study, we explore the model in the bare parameter space, varying the lattice coupling and bare mass. Simulations are carried out with three colors and 12 flavors of dynamical staggered fermions in the fundamental representation. The analysis of the chiral order parameter and the mass spectrum of the theory indicates the restoration of chiral symmetry at zero temperature and the presence of a Coulomb-like phase, depicting a scenario compatible with the existence of an infrared stable fixed point at nonzero coupling. Our analysis supports the conclusion that the onset of the conformal window for QCD-like theories is smaller than $N_f = 12$, before the loss of asymptotic freedom at 16 and 1/2 flavors. We discuss open questions and future directions.

DOI: 10.1103/PhysRevD.82.074503 PACS numbers: 11.15.Ha, 11.10.Hi, 11.25.Hf, 11.30.Rd

I. INTRODUCTION

With the imminent activity of the LHC experiments and the quest for a theory describing fundamental forces beyond the electroweak symmetry breaking scale, renewed interest has arisen in the most elusive aspects of gauge theories. In particular, the possibility of an emergent quasiconformal symmetry in theories with fermionic content has attained a strong experimental appeal. There are multiple reasons for pursuing this search. Resolving conformal behavior would complete our understanding of the phase diagram of gauge theories by varying temperature and number of flavors, as sketched in Fig. 1. It sheds light on how the low temperature and large flavor number quasiconformal phase may be connected to the high temperature and low flavor number quark-gluon plasma phase. It is essential for theoretically establishing or excluding walking technicolor-type theories and more generally strongly interacting dynamics above the electroweak symmetry breaking scale. Finally, elucidating the way conformal symmetry or its remnants drive the dynamics of particle interactions with or without supersymmetry contributes to clarifying the possible connection of field theory to string theory that the AdS/CFT correspondence seems to imply.

In the early eighties, our understanding of the perturbative behavior of non-Abelian gauge theories was enriched by two seminal papers [1,2]. It was noticed that a second zero of the two-loop beta function of an SU(3) gauge theory with N_f massless fermions in the fundamental representation appears for $N_f \gtrsim 8.05$, at $g^{*2} \neq 0$, before the loss of asymptotic freedom at $N_f^c = 16\frac{1}{2}$. This fact implies, at least perturbatively, the appearance of an infrared fixed point (IRFP). The fixed point moves closer to zero coupling as the number of flavors approaches N_f^c. The dynamics of chiral symmetry have led to the discovery of the conformal window in QCD-like theories [3,4]: chiral symmetry breaking can only occur below a critical number of flavors N_f^*. Between N_f^* and N_f^c, the conformal window opens up. Finding the actual value of the critical number of flavors N_f^* at which chiral symmetry breaking takes place is a nonperturbative problem for which the lattice approach is the method of choice [5]. Recent studies have provided evidence that $N_f = 8$ lies within the hadronic phase of QCD [6–10]. A recent study of the SU(3) running coupling [6,9] by use of the lattice Schrödinger functional has concluded that $N_f = 12$ should already be in the conformal window. Other numerical studies, however, challenged this conclusion [11–13]. This is hardly surprising, given that $N_f = 12$ should be very close to the critical number of

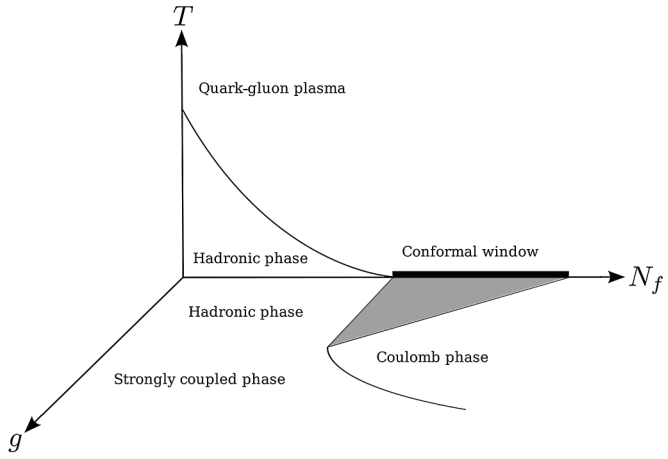

FIG. 1. A projected view of the phase diagram of QCD-like theories in the temperature (T), flavor number (N_f), and bare coupling (g) space. In the T-N_f plane, the critical line is a phase boundary between the chirally broken hadronic phase and the chirally symmetric quark-gluon plasma, the zero temperature end point of which is the onset of the conformal window. The zero temperature projected plane is inspired by the scenario in Refs. [3,4], see Fig. 2.

 © 2010 The American Physical Society

flavors [14–17], making a numerical study particularly delicate.

The current strategy, complementary to that of Refs. [6,9], is inspired by the physics of phase transitions; it allows for the exploration of multiple aspects of the theory in different regimes and regions of the phase diagram, in order to probe the existence and properties of an IRFP inside and outside its basin of attraction.

This paper is organized as follows. In Sec. II, we review previous theoretical work, in particular, the scenario for conformality originally proposed in Refs. [3,4], and define our strategy. Section III shortly describes the simulations and the observables of this work. Section IV presents the results on the bulk chiral phase transition, while Sec. V further discusses the behavior of the chiral order parameter. Here, several subsections describe various theoretically motivated models, and related fits for the mass dependence of the chiral condensate. Section VI addresses the spectrum, and it is organized in two subsections. The first one discusses the interrelation between the spectrum results and the pattern of chiral symmetry. The second subsection, similar in spirit to Ref. [18], argues that the lattice spacing increases when decreasing the coupling, as expected of a negative beta function; finally, it uses the numerical results combined with the perturbative input to argue in favor of the existence of a zero of the beta function. In Sec. VII, we summarize the results, draw our conclusions, and briefly discuss future directions.

II. A SCENARIO FOR CONFORMALITY AND A LATTICE STRATEGY

The strategy of this study has received heuristic guidance from the scenario depicted in Refs. [3,4] and sketched in Fig. 2.

The zero temperature phase diagram of Fig. 2, originally proposed in Ref. [4], is of course conjectural at this stage: even the existence of the conformal window itself needs to be verified by an *ab initio* calculation. The scenario is based on analytic, necessarily approximate estimates, and *ab initio* lattice studies are also needed to clarify the shape and nature of the various lines. Importantly, the line of IRFP is not a phase transition in the scenario of Ref. [4], while it is a chiral transition in the one of Ref. [2], known as the Banks-Zaks scenario. The shape of the line of IRFP is of course scheme dependent. The nature of the phase transitions on each line of Fig. 2, in particular, on the bulk transition line—which is relevant in the context of the search for an ultraviolet fixed point (UVFP) at strong coupling—and the way the lines merge depend on the details of the dynamics. This is why it is important to carry out a lattice study.

For our present scope, it suffices to bear in mind that a conformal window, if any, should be preempted by a zero temperature lattice chirally symmetric phase. This is

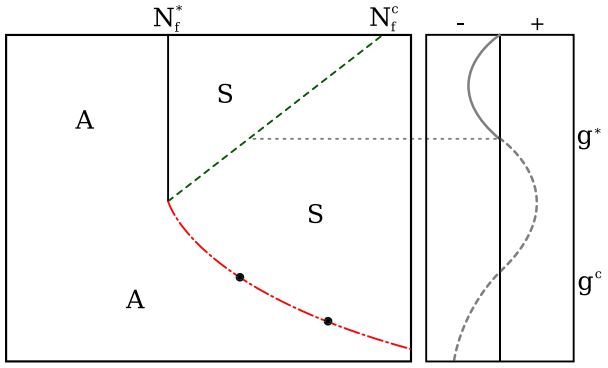

FIG. 2 (color online). Phase diagram of an SU(3) gauge theory with fundamental fermions in the number of flavors N_f—bare coupling g plane after Ref. [4]. Theories for $N_f < N_f^*$ are QCD-like in the continuum. For $N_f^* < N_f < N_f^c$, theories develop a conformal phase. S and A refer to chirally symmetric and asymmetric, respectively. The dashed (green) line qualitatively indicates the location of the Banks-Zaks IRFP [2]. The dot-dashed (red) line indicates a lattice bulk transition, which has been observed at $N_f = 12$ and $N_f = 16$. The line at $N_f = N_f^*$ represents the conformal phase transition [3,4], which is absent in the original Banks-Zaks scenario. The beta function on the conformal side is also sketched.

a robust feature, which does not depend on any of the interesting details of the phase diagram outlined above.

We will implicitly assume the validity of that scenario in the lattice bare coupling g space, where we shall work in the rest of this paper.

On the weak coupling side of Fig. 2, for any $N_f < N_f^c$, the continuum limit exists for $g \to 0$, due to asymptotic freedom. Should the IRFPs and the conformal window exist, the corresponding lines in Fig. 2 have a mapping onto the phase diagram of the continuum theory. We add that, if an UVFP at strong coupling [19] exists, the line of bulk transitions signals the emergence of a new continuum limit on the strong coupling side of Fig. 2. The existence of UV fixed points at strong coupling in four dimensions is a long-standing problem in field theory. Second order phase transitions at strong coupling are natural candidates for such fixed points. Their nontrivial critical dynamics could signal the emergence of an interacting theory, distinct from the asymptotically free dynamics of QCD.

Following Fig. 2, at a given $N_f > N_f^*$ and increasing the coupling from $g = 0$, one crosses the conformal line, location of the IRFPs, going from a chirally symmetric (S) and asymptotically free phase (quasiconformal phase) to a symmetric, but not asymptotically free one (Coulomb-like or QED-like phase). A phase transition need not be associated with the line of IRFPs, differently from what was originally speculated in Ref. [2]. At even larger couplings, a transition to a strongly coupled chirally asymmetric (A) phase will always occur in the lattice regularized theory. The latter is referred to as a bulk phase transition. In the symmetric phases at nonzero coupling, the conformal

symmetry is still broken by ordinary perturbative contributions. They generate the running of the coupling constant which is different on the two sides of the symmetric phase. See Ref. [4] for a detailed discussion of this point. We emphasize that in the region considered in this paper, conformal symmetry would still be broken by Coulombic forces.

A theory in the hadronic phase, $N_f < N_f^*$, has a thermal phase transition in the continuum from a low temperature chirally broken phase to a high temperature chirally symmetric—quark-gluon plasma—phase. Thus, as argued in Ref. [7], the observation of a thermal transition in the continuum limit is incompatible with the existence of a conformal fixed point, see Fig. 1. It is also clear from Fig. 2 that the presence of a Coulomb-like phase next to the bulk transition at weaker coupling is a distinguishing feature of the conformal phase. Here, the nonperturbative beta function should be positive, implying a weakening of the effective coupling over increasing distances. The appearance of such a region is, in principle, a sufficient condition for the existence of an IRFP, since the perturbative beta function of SU(3) with $N_f < 16\frac{1}{2}$ in the extreme weak coupling regime is known to be negative. Note, however, that the beta function is not universal away from fixed points with diverging correlation lengths, and one can therefore not exclude *a priori* the appearance of spurious fixed points at intermediate values of the coupling constant [18]. The reader should keep in mind that we will work with a lattice beta function; please see Sec. VI B for a caveat and discussions of this point.

The evidence presented here thus consists of a few components. First, it will be demonstrated that the location of the transition from the chirally symmetric to the broken phase is not sensitive to the physical temperature and is therefore compatible with a bulk nature. Subsequently, we will present a detailed study of the mass dependence of the chiral condensate on the weak coupling side of the bulk transition, which clearly favors exact chiral symmetry. Finally, the behavior of the mass spectrum close to the bulk transition will be studied and found to be compatible with a positive beta function, similarly to the observations of Ref. [18] for $N_f = 16$, and the restoration of chiral symmetry. These results are consistent with the scenario for conformality of Fig. 2.

III. THE SIMULATIONS AND THE OBSERVABLES

We have simulated an SU(3) gauge theory with 12 flavors of staggered fermions in the fundamental representation. We used a tree-level Symanzik improved gauge action to suppress lattice artifacts, and Kogut-Susskind (staggered) fermions with the Naik improvement scheme, that effectively extends the Symanzik improvement to the matter content.

High statistics runs were performed at fixed bare quark mass $am = 0.05$ over an extended range of bare lattice couplings, on $16^3 \times 8$ and 16^4 lattices. At two selected couplings, $6/g_L^2 = 3.9$ and $6/g_L^2 = 4.0$, we have performed runs on lattices $20^3 \times 32$, 24^4, 32^4 and five masses $am = 0.025$, 0.04, 0.05, 0.06, 0.07. The thermalization of all runs was extensively verified by monitoring the stability of averages and uncertainties as a function of the discarded number of sweeps and bin size. In addition, we have verified the decorrelation from initial conditions by performing simulations with ordered and random starts for a few selected couplings and masses.

We have measured gauge and fermionic observables including the average plaquette, the Polyakov loop, the interquark potential, the chiral condensate, and its susceptibility, the meson spectrum. We report here on our results for the chiral condensate and the meson spectrum. We underscore that staggered fermions have a remnant of exact chiral symmetry which allows a precise definition of the chiral order parameter—the condensate $\langle \bar{\psi}\psi \rangle$—also on a coarse lattice.

IV. THE BULK TRANSITION

Figure 3 shows our results for the chiral condensate at a fixed value of the bare quark mass $am = 0.05$ and for two volumes $16^3 \times 8$ and 16^4, differing by a factor of 2 in their temporal extent N_t. The results display a sudden variation of the chiral order parameter as a function of the bare lattice coupling constant g_L, for both N_t. At this point, one notices that the temperature of the system is related to the lattice temporal extent as $T = 1/a(g_L)N_t$, with $a(g_L)$ the lattice spacing for a given lattice coupling. From Fig. 3, one infers that the phase transition—or rapid crossover—happens at identical values of the critical coupling $g_L^c = 1.35(3)$, thus implying they occur at vastly different physical temperatures. Hence, one concludes that the observed transition (or crossover) is driven purely by the bare coupling constant itself and is therefore of bulk nature.

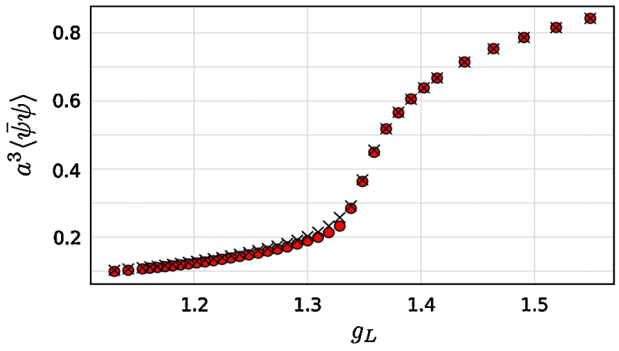

FIG. 3 (color online). The bulk transition in the chiral condensate for $am = 0.05$ on lattices of $16^3 \times 8$ (circles), and 16^4 (crosses) as a function of the bare lattice coupling g_L. Data are shown in the range $6/g_L^2 = 2.5$ to 4.7. The location of the transition is identical, while the curves describe physics at temperatures differing by a factor of 2. Simulation errors are within symbol size.

Further information on this behavior, with a refined scaling study, might shed light on the occurrence of a conjectured ultraviolet fixed point at strong coupling in the continuum theory [19].

The results of Fig. 3 beg for a detailed analysis of the behavior of the chiral condensate at weaker couplings, in order to discriminate between a genuine phase transition to a chirally symmetric phase, and a rapid crossover to a phase where chiral symmetry is still broken.

V. THE CHIRAL CONDENSATE AT $6/g_L^2 = 3.9$ AND $6/g_L^2 = 4.0$

In order to be able to extract information on the symmetry of the vacuum—chiral symmetry broken or restored—by extrapolating the condensate to the chiral limit, we need to measure it at infinite volume and at sufficiently light values of the quark masses. Light here means that the dynamics of the system is not yet dominated by the amount of explicit chiral symmetry breaking. This study, being of course extremely demanding from the point of view of numerical resources, was performed for two relevant selected couplings. We will first address the issue of systematic errors; then, we will consider and compare several theoretically motivated parameterizations, appropriate for chirally broken or symmetric phases.

A. Aspects of systematics

To reach the infinite volume limit within statistical errors, measurements of the chiral condensate were performed on three different volumes for each mass, up to 32^4 for the smallest masses, and the difference between the largest two volumes found to be smaller than both the difference between the smallest volumes and the statistical uncertainty in all measurements, as can be gleaned from Fig. 4 and Table I. The data set used for the extrapolation to the chiral limit thus consists of the measurements at lattice volumes 24^4, which can be considered as infinite volume measurements within their errors, again according to Fig. 4 and Table I.

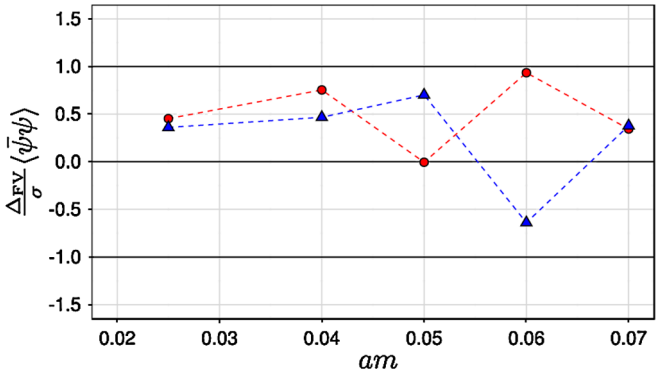

FIG. 4 (color online). Observed finite volume effects in the chiral condensate, displayed as the difference Δ_{FV} between the measurements at the two largest available volumes ($24^3 \times 24$ and $32^3 \times 32$ for the lowest mass, $20^3 \times 32$ and $24^3 \times 24$ for the other masses) divided by their combined standard deviation σ. Blue triangles indicate results for $6/g_L^2 = 3.9$, red circles those for $6/g_L^2 = 4.0$. A value of less than unity (within the band) implies that finite volume effects are within a single standard deviation of each other and therefore statistically irrelevant.

TABLE I. Comparison of the measured chiral condensate at different volumes, with varying bare masses am and for two lattice couplings $6/g_L^2 = 3.9$ and 4.0. For all masses, the measurements at volume $N_s \times N_t = 24^3 \times 24$ differ from the adjacent volumes by less than their statistical uncertainty. We therefore use the 24^4 measurements as input to the chiral extrapolations of Table VI.

$6/g_L^2$	am	$a^3\langle\bar{\psi}\psi\rangle_{N_s=20}$	$a^3\langle\bar{\psi}\psi\rangle_{N_s=24}$	$a^3\langle\bar{\psi}\psi\rangle_{N_s=32}$
3.9	0.025	0.07638(22)	0.07693(07)	0.07697(07)
	0.040	0.12107(10)	0.12092(17)	
	0.050	0.15018(17)	0.15018(10)	
	0.060	0.17918(17)	0.17897(14)	
	0.070	0.20776(19)	0.20768(10)	
4.0	0.025	0.07212(13)	0.07202(10)	0.07206(05)
	0.040	0.11366(09)	0.11360(10)	
	0.050	0.14093(19)	0.14079(07)	
	0.060	0.16775(16)	0.16787(11)	
	0.070	0.19476(11)	0.19470(13)	

Evidence that we are considering sufficiently light quark masses is provided by the mass dependence of the condensate itself, and by our results for the spectrum in Sec. VI, where we further elucidate this aspect.

As for the issue of the continuum limit, we remind the reader that all the measurements are performed at a fixed value of the lattice spacing and no extrapolation to the continuum limit is considered. On the other hand, in the scenario of Fig. 1, there is only one symmetric phase at large N_f. Hence, once chiral symmetry is restored, it should stay so till the continuum. A preliminary study towards weak coupling has revealed no sign of further phase transitions, thus confirming this scenario. Being notoriously difficult to directly probe the IRFP with a lattice study, we are collecting precisely those measurements at finite lattice spacing and varying lattice coupling that can provide a combined evidence for the restoration of chiral symmetry and for the existence of the peculiar non asymptotically free regime that precedes the IRFP for decreasing coupling, a feature proper to non-Abelian gauge theories with a conformal phase.

B. Fits motivated by a possible Goldstone phase

The functional forms discussed here would be appropriate if the bulk behavior were not to be associated to a true chiral transition. For instance, it might just be due to a generic rapid crossover, or to a genuinely lattice transition between two phases with different ordering. In this case,

TABLE II. Fits to $\langle\bar{\psi}\psi\rangle = Am + Bm\log m + \langle\bar{\psi}\psi\rangle_0$.

$6/g_L^2$	A	B	$\langle\bar{\psi}\psi\rangle_0$	$\sqrt{\chi^2\text{dof}}$
3.9	2.70(3)	−0.103(13)	0.00013(54)	0.68
	3.12(3)	0 (F)	0.0043(3)	3.12
	2.682(5)	−0.107(2)	0 (F)	0.56
4.0	2.48(2)	−0.120(10)	−0.00091(42)	0.51
	2.73(1)	0 (F)	0.0041(5)	3.74
	2.519(8)	−0.099(3)	0 (F)	0.56

the range of couplings between $6/g_L^2 = 3.9$ and $6/g_L^2 = 4.0$ would still belong to the phase with broken chiral symmetry. We have thus considered the following functional form,

$$\langle\bar{\psi}\psi\rangle = Am + Bm\log(m) + \langle\bar{\psi}\psi\rangle_0, \tag{1}$$

where the parameters were all left free, giving fits with 2 degrees of freedom, or in turn constrained to zero. The logarithmic mass dependence is typical of a chirally broken phase for a QCD-like theory in four dimensions at zero temperature.

The results of the fits to Eq. (1) are summarized in Table II. The linear fits—case $B = 0$ also used in [13]—produce an intercept different from zero, but are highly disfavored by their large χ^2. The inclusion of the term $m\log(m)$ considerably improves the quality of the fits. Those with free intercept $\langle\bar{\psi}\psi\rangle_0$ gave an extrapolated value consistent with zero, and in agreement with the fit obtained by constraining $\langle\bar{\psi}\psi\rangle_0 = 0$. Both fits are satisfactory and imply that the chiral condensate in the chiral limit is zero within errors. In conclusion, a conventional picture of the Goldstone phase seems not to be supported by our data.

C. Fits with an anomalous dimension

We considered the functional form

$$\langle\bar{\psi}\psi\rangle = Am^{1/\delta} + Bm + \langle\bar{\psi}\psi\rangle_0, \tag{2}$$

containing an anomalous dimension, whose effect is parameterized by the exponent δ. Since the fits described in Sec. V B already suggest that a curvature in the behavior of the chiral condensate as a function of the mass is mandatory, we started by setting the linear term to zero. We note that analogous fits were used in the past to analyze QED in its symmetric phase, close to the strong coupling transition in Ref. [20], even if a more satisfactory account of the data requires the consideration of the magnetic equation of state, which is going to be discussed in the next section. Results for these fits are reported in Table III. All fits to Eq. (2) with $B = 0$ are satisfactory, with a chiral condensate compatible with zero in the chiral limit. This was checked, as before, by comparing fits with free intercept, and fits with $\langle\bar{\psi}\psi\rangle_0 = 0$.

One might still suspect that a fit combining a power-law term and a linear term, with a nonzero intercept might still accommodate the data, hence indicating chiral symmetry breaking. For instance, a linear term can arise because of the additive renormalization of the chiral condensate—see, e.g., [21] for a discussion of this term in the context of the QCD thermal transition.

TABLE III. Fits to $\langle\bar{\psi}\psi\rangle = Am^{1/\delta} + Bm + \langle\bar{\psi}\psi\rangle_0$.

$6/g_L^2$	A	$1/\delta$	B	$\langle\bar{\psi}\psi\rangle_0$	$\sqrt{\chi^2\text{dof}}$
3.9	3.00 (F)	0.960 (F)	−0.30 (F)	−0.00002 (F)	0.96
	2.700 (4)	0.9646 (4)	0.00 (F)	0.0000 (F)	0.55
	2.699 (25)	0.964 (4)	0.00 (F)	−0.0000 (6)	0.68
	1.86 (24)	0.950 (F)	0.83 (26)	−0.0001 (5)	0.68
	2.10 (27)	0.955 (F)	0.60 (29)	−0.0001 (6)	0.68
	2.38 (30)	0.960 (F)	0.31 (33)	−0.0001 (5)	0.68
	2.75 (35)	0.965 (F)	−0.05 (38)	−0.0000 (1)	0.68
	3.24 (41)	0.970 (F)	−0.54 (44)	−0.0000 (5)	0.68
	3.93 (50)	0.975 (F)	−1.23 (53)	0.0000 (5)	0.69
	4.97 (64)	0.980 (F)	−2.27 (66)	0.0000 (6)	0.68
4.0	1.230 (F)	0.910 (F)	1.26 (F)	−0.0010 (F)	0.70
	2.534 (8)	0.965 (1)	0.00 (F)	0.0000 (F)	0.87
	2.489 (18)	0.956 (3)	0.00 (F)	−0.0011 (4)	0.51
	2.15 (17)	0.950 (F)	0.33(18)	−0.0011 (4)	0.50
	2.42 (19)	0.955 (F)	0.06(21)	−0.0012 (4)	0.51
	2.76 (21)	0.960 (F)	−0.26(23)	−0.0011 (4)	0.51
	3.18 (25)	0.965 (F)	−0.70(27)	−0.0011 (4)	0.51
	3.75 (30)	0.970 (F)	−1.26(32)	−0.0011 (4)	0.51
	4.55 (36)	0.975 (F)	−2.06(38)	−0.0010 (4)	0.52
	5.74 (45)	0.980 (F)	−3.26(47)	−0.0010 (4)	0.52

For completeness, we have performed fits to Eq. (2) with the inclusion of a linear term. As expected from the near degeneracy between a power law with $1/\delta \approx 1$ and a linear term, the uncertainties coming from a Marquardt-Levenberg minimization of χ^2 are huge, ranging from 100% to 10 000%. In Table III, we simply quote the central results, omitting the errors. Studies able to disentangle the effect of linear scaling violations [21] were using an exact form for the scaling function which is not available here. In conclusion, the behavior of the fits to Eq. (2) says that an additional linear term, or any analytic term in Eq. (2), is redundant for our data.

To acquire a feeling about the possible relevance of a linear term, we have also performed a sequence of fits, constraining the exponent to several values in the acceptable range given by the fit errors. The results are again summarized in Table III. It appears that the coefficient of the linear term smoothly changes from positive to negative, while the intercept—the chiral condensate in the chiral limit—remains consistent with zero throughout at $6/g_L^2 = 3.9$, and becomes slightly negative at $6/g_L^2 = 4.0$. We thus again conclude that our data point at exact chiral symmetry.

D. Fits motivated by the magnetic equation of state

Finally, we considered fits motivated by the magnetic equation of state. The following equation is a satisfactory parameterization

$$m = A\langle\bar{\psi}\,\psi\rangle + B\langle\bar{\psi}\,\psi\rangle^{\delta}, \tag{3}$$

which would of course coincide with the simple power law when $A = 0$. The coefficient of the linear term A should vanish at a critical point, with $A \propto (\beta - \beta_c)$. This of course explains the smallness of A close to the transition, while δ is the conventional magnetic exponent. The linear term in the condensate is implied by chiral symmetry, and guarantees that the ratio

$$\lim_{m\to 0} R_\pi = \frac{\partial\langle\bar{\psi}\,\psi\rangle/\partial m}{\langle\bar{\psi}\,\psi\rangle/m} = 1 \tag{4}$$

approaches unity in the chiral limit and in the chirally symmetric phase. We can view Eq. (3) as a model for a theory with anomalous dimensions, which incorporates the correct chiral limit. Note that the linear term of Eq. (3) is of different origin than the one considered in Eq. (2). The latter describes violations of scaling and it is increasingly relevant at larger masses. In Eq. (3) instead, it is dominating at very small masses, away from the critical point.

TABLE IV. Fits to $m = A\langle\bar{\psi}\,\psi\rangle + B\langle\bar{\psi}\,\psi\rangle^{\delta}$.

$6/g_L^2$	A	B	δ
3.9	0.1(9)	0.3(9)	1.1(2)
4.0	0.3(1)	0.077(9)	1.3(1)

TABLE V. Comparison of the simulation results for $\langle\bar{\psi}\,\psi\rangle$ with the ones obtained from the fits to the magnetic equation of state.

$6/g_L^2$	am	$\langle\bar{\psi}\,\psi\rangle$	$\langle\bar{\psi}\,\psi\rangle_{\rm fit}$
3.9	0.025	0.07693(07)	0.07689
	0.040	0.12092(17)	0.12102
	0.050	0.15018(10)	0.15010
	0.060	0.17897(14)	0.17898
	0.070	0.20768(10)	0.20768
4.0	0.025	0.07202(10)	0.07204
	0.040	0.11360(10)	0.11355
	0.050	0.14079(07)	0.14083
	0.060	0.16787(11)	0.16787
	0.070	0.19470(13)	0.19469

Results for this case are given in Table IV. The fit $m = m(\langle\bar{\psi}\,\psi\rangle)$ was performed with a least squares algorithm. Note that, as expected, the significance of the linear term is very low, closer to the bulk transition, and slightly larger by moving away from it. In Table V, we quote the numerical solutions of the equation $m(\langle\bar{\psi}\,\psi\rangle) = m_{\rm sim}$, with $m_{\rm sim}$ the simulation masses, to be compared with the simulation results for the condensate. The agreement is very good.

All fits clearly favor a positive value for the coefficient of the linear term, as it should be in the chirally symmetric phase, and within the large errors, the results for the exponent are compatible with the ones coming from the genuine power-law fits. We conclude again in favor of chiral symmetry restoration.

E. Side-by-side comparison of the two simplest scenarios

The spirit of the analysis performed above is to see if any of the simplest physically motivated parameterizations can account for a condensate in the chiral limit different from zero, and we can conclude that all analyses favor a vanishing chiral condensate. In this subsection, we directly compare in more detail the genuine linear fit, Eq. (1) with $B = 0$, as this is the only fit that produced a tiny nonzero chiral condensate, and the genuine power-law fit, Eq. (2) with B and $\langle\bar{\psi}\,\psi\rangle_0 = 0$, being the simplest fit with a χ^2 in an acceptable statistical range. In the rest of this section, we refer to these fits as ''linear'' and ''power law,'' respectively.

The measured values of the chiral condensate and those predicted by the linear and power-law fits are shown in Table VI. In Fig. 5, the measured data with superimposed fits are shown. Of course, since the range of variability of the chiral condensate is exceedingly larger than its errors, it is impossible to appreciate by eye the quality of the fits on this scale. A more effective description of the relative quality of the fits is offered by Figs. 6 and 7 . In Fig. 6, we plot the difference between the chiral condensate predicted by the fits and the data, divided by the data

TABLE VI. Measurements of the chiral condensate at $N_s \times N_t = 24^3 \times 24$ for two values of the coupling $6/g^2 = 3.9$ and 4.0, and a range of bare quark masses am, together with the values predicted by the fits to a linear and a power-law model.

$6/g_L^2$	am	$a^3\langle\bar{\psi}\psi\rangle_{\text{measured}}$	$a^3\langle\bar{\psi}\psi\rangle_{\text{linear}}$	$a^3\langle\bar{\psi}\psi\rangle_{\text{power}}$
3.9	0.025	0.07693(07)	0.07705	0.07692
	0.040	0.12092(17)	0.12069	0.12105
	0.050	0.15018(10)	0.14978	0.15013
	0.060	0.17897(14)	0.17887	0.17899
	0.070	0.20768(10)	0.20796	0.20769
4.0	0.025	0.07202(10)	0.07237	0.07212
	0.040	0.11360(10)	0.11331	0.11350
	0.050	0.14079(07)	0.14060	0.14077
	0.060	0.16787(11)	0.16789	0.16785
	0.070	0.19470(13)	0.19518	0.19477

themselves. The tension between fitted and numerical results for the linear form is quite evident. The pattern of the deviations in the linear fits indicates a significant curvature, which is reflected in the quality of the fit. The pattern of the residuals of the power-law fit is instead far less structured and statistically insignificant throughout. Figure 7 offers in our opinion the most clear way of visualizing the deviations by plotting the same difference as in Fig. 6, this time divided by the error σ. The horizontal band indicates the boundary of 1 standard deviation, and the points obtained by a power-law fit nicely fall within it, while again the tension with the linear form appears. These results thus confirm a strong preference for the restoration of chiral symmetry at the weak coupling side of the transition, as was inferred from Sec. V A to Sec. V D.

It is clear that additional data at even lighter masses will improve the discriminating power of these fits and eventually allow to significantly constrain the linear contributions. The presence of curvature in the data and the very good quality of the power-law fit, having barred finite volume effects, is also an indication that we are not in the heavy quark limit. In addition, one could also study the analogous of the Gell-Mann-Oakes-Renner (GMOR) relation of broken chiral symmetry, and variations of it in terms of the scalar meson mass, by also measuring the pion decay constant f_π in the chiral limit and the scalar mass.

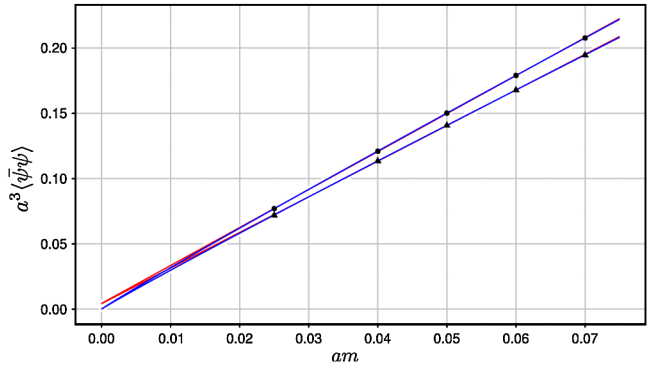

FIG. 5 (color online). Fits to the chiral condensate measured at $6/g_L^2 = 3.9$ (circles) and $6/g_L^2 = 4.0$ (triangles), with linear fits shown in red and power-law fits (going through the origin) drawn in blue.

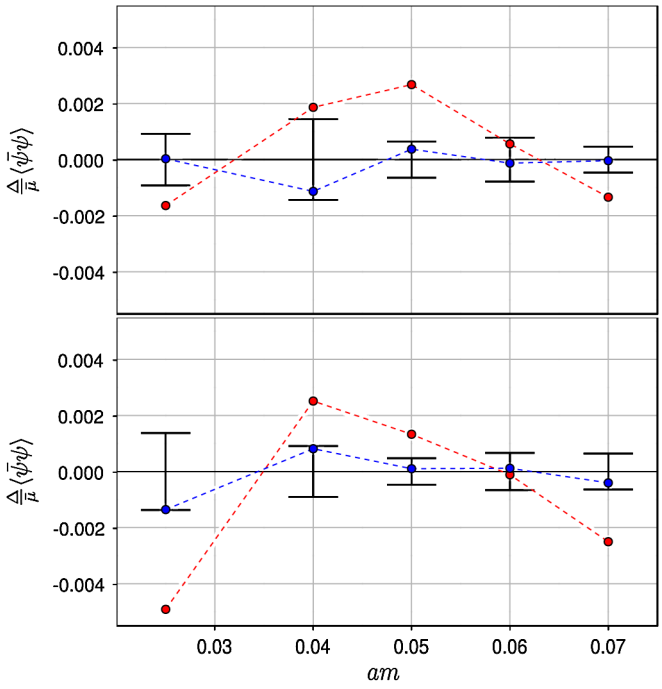

FIG. 6 (color online). Deviations Δ of the fitted value from the measured value $\bar{\mu}$ for the chiral condensate, rescaled by the measured value itself. Error bars represent the relative (rescaled by the data) standard deviation on the measured value. Deviations from the prediction with a fit to the linear form are given in red, while those for a fit to a power-law (smallest deviations) are given in blue. The top graph displays results for $6/g_L^2 = 3.9$, the lower graph those for $6/g_L^2 = 4.0$. The linear form shows tension with the data for both values of the coupling, which is quantitatively seen in the larger χ^2 value.

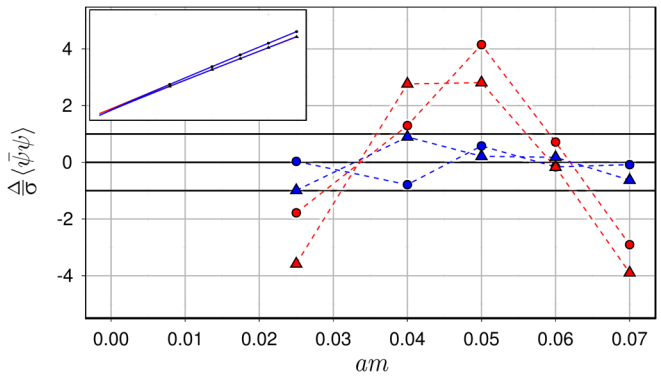

FIG. 7 (color online). Deviations Δ of the fitted value from the measured one for the chiral condensate, rescaled by the standard deviation σ of each measurement. Results are shown for both $6/g_L^2 = 3.9$ (circles) and $6/g_L^2 = 4.0$ (triangles), with fits to the linear form shown in red and fits to the power law (smallest deviations) drawn in blue. The data and corresponding fits are displayed on linear scales in the inset.

VI. SPECTRUM ANALYSIS

An alternative approach to the study of the symmetry of a phase is offered by the spectrum analysis [22]. Particularly useful quantities for this type of study are the masses of the ground state excitations in the pseudoscalar and vector channels, with slight abuse of nomenclature from QCD referred to as the π and ρ masses. We defer to future work the exploration of other interesting observables, such as the ratio of the scalar and pseudoscalar masses or equivalently the ratio of transverse and longitudinal chiral susceptibilities.

A. Spectrum and chiral symmetry

A powerful way to distinguish between symmetric and broken chiral symmetry [22] is to plot the pseudoscalar mass as a function of the chiral condensate, as in Fig. 8. We have considered the same range of bare fermion masses used in Sec. V for the chiral extrapolation of the condensate. The data are best fitted by a simple power-law form, and the results are reported in Table VII. They clearly suggest that chiral symmetry is restored and that the theory has anomalous dimensions. In the symmetric phase and in mean field [22], we expect a linear dependence with nonnegative intercept. The presence of anomalous dimensions is responsible for negative curvature—noticeably opposite to what finite volume effects would induce—and a zero intercept. The same graph in the broken phase would show the opposite curvature and extrapolate with a negative intercept.

This result gives also further confidence that the fermion masses used in this study are not too light so that they do not significantly feel the finite volume, and not too heavy so that they are not blind to chiral symmetry. In Fig. 9, we report on the measured values of m_π and m_ρ as a function of the bare fermion mass. Here, the lightest point at $am = 0.025$ for the vector mass is absent, but a curvature can still be appreciated. Simulations were done on $16^3 \times 24$ volumes, while a set of measurements at larger volumes showed that finite volume effects were under control. The mass dependence shown in Fig. 9 hints again at a few properties of a chirally symmetric phase. We have fitted both the pion and the rho mass to a power law

$$m_{\pi,\rho} = A_{\pi,\rho} m^{\epsilon_{\pi,\rho}} \tag{5}$$

with the results $A_\pi = 3.41(21)$, $\epsilon_\pi = 0.61(2)$, $A_\rho = 4.47(61)$, $\epsilon_\rho = 0.66(5)$ at $6/g_L^2 = 3.9$, and $A_\pi = 3.41(21)$, $\epsilon_\pi = 0.61(2)$, $A_\rho = 4.29(11)$, $\epsilon_\rho = 0.66(1)$ at $6/g_L^2 = 4.0$. The accuracies of these fits are not comparable with those achieved by the fits to the chiral condensate; however, they allow to draw a few conclusions. First, the mass dependence of the vector and pseudoscalar mesons is well fitted by a power law. Second, it is also relevant that the exponents are not unity and $\epsilon_\pi \neq 1/2$. The latter result immediately tells that the pion seen here is not a Goldstone boson of a broken chiral symmetry. In addition, both mesons have masses scaling with roughly the same power, as it should be in a symmetric phase, and with

TABLE VII. Results of fits to the functional form $(am_\pi)^2 = A(a^3\langle\bar\psi\,\psi\rangle)^{2\delta_\chi}$. Fits are performed to the separate values of the coupling constant and the combined data set.

$6/g_L^2$	parameter	value
3.9	A	3.350(70)
	δ_χ	0.639(6)
	$\sqrt{\chi^2\text{dof}}$	0.73
4.0	A	3.500(40)
	δ_χ	0.649(3)
	$\sqrt{\chi^2\text{dof}}$	0.46
combined	A	3.400(50)
	δ_χ	0.642(4)
	$\sqrt{\chi^2\text{dof}}$	0.70

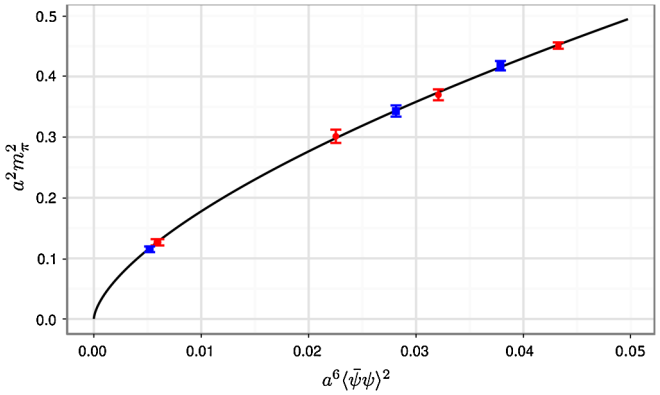

FIG. 8 (color online). The relation between the chiral condensate and the pion mass, for $6/g_L^2 = 3.9$ (blue squares) and 4.0 (red circles). The line represents a power law fit to the combined data, the results of which are reproduced in Table VII.

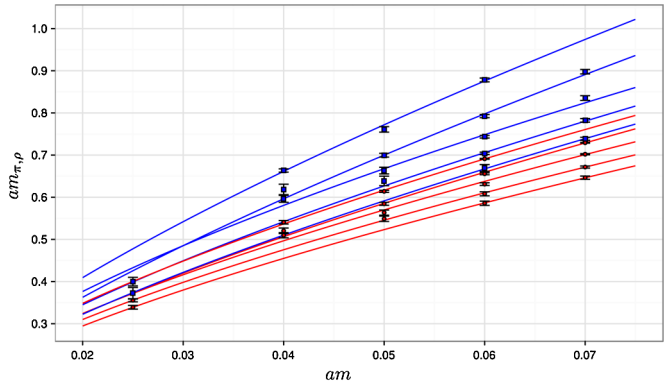

FIG. 9 (color online). The relation between the bare quark mass and the masses of the pion (red circles) and rho meson (blue squares), for $6/g_L^2 = 3.6$, 3.7, 3.8, 3.9, and 4.0 from the uppermost line down. Power-law fits to the separate values of beta are provided.

increasing degeneracy towards the chiral limit. The exponent of the power law being not one, confirms that we are not in the heavy quark regime.

These results are confirmed in a more visual way by looking at the behavior of the mass ratio. Figure 10(b) shows the ratios of measured pseudoscalar and vector masses, for a fixed coupling and as a function of the bare quark mass. We have superimposed the ratios of the best fits to the raw mass data, as explained in Sec. VI B. It is immediately clear that the ratio increases as the quark mass approaches zero, a behavior opposite to what is expected for a Goldstone pion. Notice also that the mass ratio should be one for exact conformal symmetry in the chiral limit: we do not yet observe that, since, as explained in Sec. II, conformal symmetry is expected to be broken by Coulombic forces in the region of parameter space probed by this study. On the other hand, the trend towards unity as decreasing the lattice coupling g_L is evident, and certainly worth further exploration. See also Ref. [23] for a study of the spectrum.

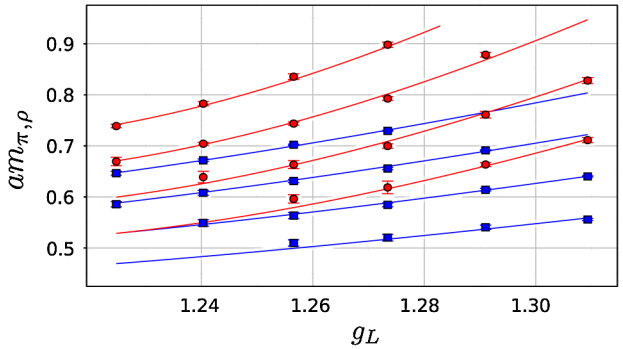

(a)Interpolations of meson masses.

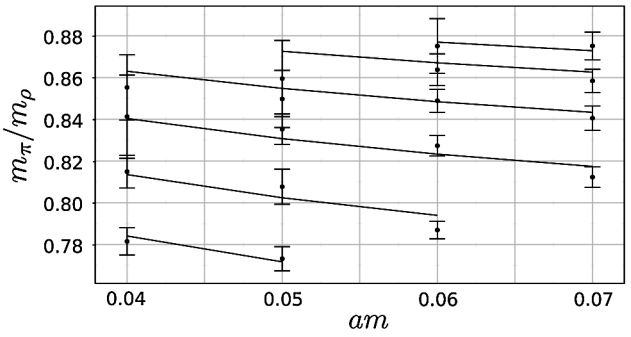

(b)π to ρ mass ratio with fits superimposed

FIG. 10 (color online). (a) Measurements of the pseudoscalar (blue) and vector (red) masses versus lattice coupling at several values of the bare quark mass, from bottom to top $am = 0.04$, 0.05, 0.06, and 0.07. Lines displayed represent a global parameterization, with a mixed $O(m)$ polynomial quark mass dependence and $O(\beta^2)$ polynomial dependence, with lattice parameter $\beta = 6/g_L^2$, and producing a reduced χ^2 per degrees of freedom just over unity for both channels. Errors include fitting systematics from combining several methods. (b) The measured π to ρ mass ratio as a function of the bare mass and decreasing coupling g_L, bottom to top $6/g_L^2 = 3.5$ to 4. The superimposed lines are ratios of the best fits in Fig. 10(a).

B. Spectrum, lattice spacing, and the beta function

We used the spectrum results to determine the lines of "constant physics" in the two dimensional parameter space g_L and am, the bare quark mass of degenerate fermions, following the same strategy which was successful for $N_f = 16$ [18]. Along these lines, the coupling and masses are all functions of the lattice spacing a. Since all dimensionful quantities measured on the lattice will be expressed in terms of the lattice spacing and will therefore vary with g_L even if they do not physically, a dimensionless quantity has to be taken as a reference. A convenient choice is the ratio of the π and ρ masses. Before continuing, let us specify that the same caveat as in Ref. [18] applies: since we are at strong coupling, there is no guarantee that the system can be described in terms of a one-parameter beta function. This implies, for instance, that the lines of "constant physics" determined by use of certain observables might not match those determined using other observables. If multiple bare couplings are needed, it might happen that the change of physics produced by changing only one bare coupling will not be compensated by a change of mass. So our lines of "constant physics" are, strictly speaking, lines of constant m_π/m_ρ ratio. We will show in the following that in order to keep this ratio constant, the bare parameters am and g_L controlling the simulations should be tuned as if we had a one-parameter, positive beta function.

In Fig. 10(a), we report on the measured values of m_π and m_ρ as a function of the bare coupling, while Fig. 10(b) shows the ratios of measured pseudoscalar and vector masses, for a fixed coupling and as a function of the bare quark mass. We have superimposed the ratios of the best fits to the raw mass data, confirming the good quality of the interpolations derived in Fig. 10(a) and used to produce Fig. 11.

It is immediately evident from Fig. 10(b) that, in order to keep the ratio constant, we should simultaneously decrease the lattice coupling g_L and increase the bare mass. These results already indicate that the lattice spacing increases while decreasing the coupling. This is the same behavior as observed for $N_f = 16$, and of the pion-to-sigma ratio in QED. It is also expected of a one-parameter beta function with a positive sign.

To refine the analysis, and express the result in terms of a physical observable, we proceed as follows. Given the ratio m_π/m_ρ at reference values of g_L and am, one can determine a value $a'm'$ at coupling g_L' in the surroundings of g_L that reproduces the same ratio and thus lies on the same line of constant physics. This is implemented by fitting the measured values of both masses to a parameterization, as shown in Fig. 10(a), then determining the isolines

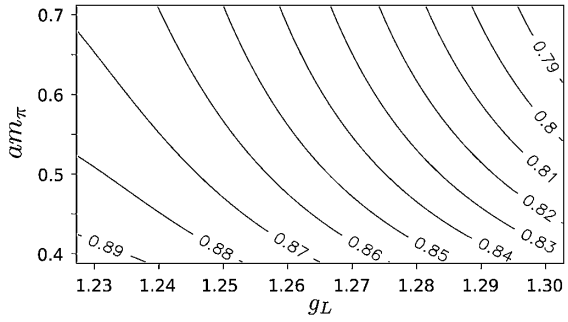

FIG. 11. Pseudoscalar mass along lines of constant physics. The physical pion mass is identical along lines of constant physics, such that a decreasing pion mass in lattice units for increasing g_L, implies an increase of the lattice spacing for weaker couplings, signature of the Coulomb-like phase. The pseudoscalar mass along lines of constant physics was constructed by interpolating along the isolines of the ratio of the separate interpolations of pseudoscalar and vector masses. Different polynomial interpolations produced compatible results, and in agreement with a noninterpolated analysis of raw data. Labels give the value of the ratio $m_\pi/m\rho$ along the isolines.

from the ratio of the two parameterizations. The physical pseudoscalar mass being constant along each of these lines, the ratio of measured values $am_\pi/a'm_\pi$ directly determines the ratio of the lattice spacings a/a'. If a decrease in g_L is associated with an increase in the lattice spacing, the sign of the beta function is positive, i.e., that of the Coulomb-like phase in Fig. 2.

Generalizing, along the lines of ''constant physics,'' the slope of the line of measured values of the pseudoscalar mass is a direct measure of the sign of the beta function. Figure 11 provides evidence for the Coulomb-like phase, with a positive sign of the beta function, in full agreement with the more naive discussion of Fig. 10. Since the beta function is known to be negative in the continuum limit, our results indicate a zero of the beta function at some intermediate coupling g. We emphasize that the location of this zero is regularization dependent, and we reiterate the caveat at the beginning of this section. Further, we do not claim to have directly studied the physics around the IRFP itself. The latter type of study is notoriously difficult, while the strategy presented here aims at probing the emergence of conformality in an indirect way.

VII. SUMMARY AND OUTLOOK

We summarize here the main findings of our study:

(i) For an SU(3) gauge theory with three unrooted staggered fermions, corresponding to 12 continuum flavors, we have observed a lattice bulk transition or crossover which is clearly of a nonthermal nature.

(ii) We have studied the realization of the chiral symmetry on the weak coupling side of this transition: the analysis of the order parameter favors chiral symmetry restoration.

(iii) A study of the spectrum in the weak coupling phase close to the transition favors chiral symmetry restoration as well.

(iv) We have derived the lines of ''constant physics'' and inferred a positive sign of the beta function, again implying the emergence of a Coulomb-like phase.

The above results provide evidence towards the existence of a symmetric, Coulomb-like phase on the weak coupling side of the lattice bulk transition. In the scenario of Refs. [3,4] and Fig. 2, such a Coulomb-like region must be entangled to the presence of a conformal infrared fixed point for the theory with 12 continuum flavors, without any further transition at weaker coupling. Such a Coulomb-like phase is not expected in ordinary QCD. We reiterate that the evidence provided is indirect, while we do not address the physics at the infrared fixed point.

A few directions are a natural extension of this work. An accurate chiral extrapolation of the chiral condensate in the strong coupling phase, would allow to determine the precise location of the chiral phase transition (or crossover). Establishing the nature of such a bulk transition might shed light on the possible emergence of an ultraviolet fixed point in the continuum theory at strong coupling [19]. It is also important to notice that a way to discriminate between the scenario of Refs. [3,4] and the one originally proposed in Ref. [2] is the presence of a chiral transition towards a broken phase at weaker couplings. While both scenarios share the presence of conformality and of a Coulomb-like phase, only in the first a range of theories exists—the conformal window—where confinement and chiral symmetry breaking do not occur at weak coupling. For a recent review on the subject, see Ref. [5]. In addition, more extended results on the mass spectrum, in particular, an analysis of the chiral partners, would shed further light on the pattern of chiral symmetry breaking and restoration for this theory. Work in these directions is in progress. Alternative studies based on the Renormalization Group analysis as proposed in [24] will provide an independent and valuable tool to investigate these systems. Such studies aim to directly probe the existence of an infrared fixed point and complement indirect searches for conformal behavior in SU(N) gauge theories with matter content.

ACKNOWLEDGMENTS

This work was in part based on the MILC public lattice gauge theory code. We thank M. Bochicchio, F. Di Renzo, J. Kuti, F. Sannino, C. deTar for comments and discussions. Computer time was provided through the Dutch National Computing Foundation (NCF) and the University of Groningen.

[1] W. E. Caswell, Phys. Rev. Lett. **33**, 244 (1974).
[2] T. Banks and A. Zaks, Nucl. Phys. **B196**, 189 (1982).
[3] T. Appelquist, J. Terning, and L. Wijewardhana, Phys. Rev. Lett. **77**, 1214 (1996).
[4] V. A. Miransky and K. Yamawaki, Phys. Rev. D **55**, 5051 (1997).
[5] E. Pallante, Proc. Sci., LAT2009 (2009) 15.
[6] T. Appelquist, G. T. Fleming, and E. T. Neil, Phys. Rev. Lett. **100**, 171607 (2008).
[7] A. Deuzeman, M. P. Lombardo, and E. Pallante, Phys. Lett. B **670**, 41 (2008).
[8] G. T. Fleming, Proc. Sci., LAT2008 (2008) 21.
[9] T. Appelquist, G. T. Fleming, and E. T. Neil, Phys. Rev. D **79**, 076010 (2009).
[10] X.-Y. Jin and R. D. Mawhinney, Proc. Sci., LAT2008 (2008) 59.
[11] Z. Fodor, K. Holland, J. Kuti, D. Nogradi, and C. Schroeder, Proc. Sci., LAT2009 (2009) 55.
[12] A. Hasenfratz, Proc. Sci., LAT2009 (2009) 52.
[13] X.-Y. Jin and R. D. Mawhinney, Proc. Sci., LAT2009 (2009) 49.
[14] T. Appelquist, A. G. Cohen, and M. Schmaltz, Phys. Rev. D **60**, 045003 (1999).
[15] J. Braun and H. Gies, J. High Energy Phys. 06 (2006) 024.
[16] T. A. Ryttov and F. Sannino, Phys. Rev. D **76**, 105004 (2007).
[17] F. Sannino, arXiv:0804.0182.
[18] P. Damgaard, U. Heller, A. Krasnitz, and P. Olesen, Phys. Lett. B **400**, 169 (1997).
[19] D. B. Kaplan, J.-W. Lee, D. T. Son, and M. A. Stephanov, Phys. Rev. D **80**, 125005 (2009).
[20] A. Kocic, S. Hands, J. B. Kogut, and E. Dagotto, Nucl. Phys. **B347**, 217 (1990).
[21] S. Ejiri *et al.*, Phys. Rev. D **80**, 094505 (2009).
[22] A. Kocic, J. B. Kogut, and M.-P. Lombardo, Nucl. Phys. **B398**, 376 (1993).
[23] L. Del Debbio, B. Lucini, A. Patella, C. Pica, and A. Rago, Phys. Rev. D **80**, 074507 (2009).
[24] T. DeGrand and A. Hasenfratz, Phys. Rev. D **80**, 034506 (2009).